ATOMOS: An ATOmistic MOdelling Solver for dissipative DFT transport in ultra-scaled HfS_2 and Black phosphorus MOSFETs

Aryan Afzalian
Imec
Kapeldreef 75, 3001 Leuven, Belgium
aryan.afzalian@imec.be

Geoffrey Pourtois
Imec
Kapeldreef 75, 3001 Leuven, Belgium
geoffrey.pourtois@imec.be

***Abstract*—A state-of-the-art DFT-NEGF based ATOmistic - MOdelling Solver (ATOMOS) was developed and used to assess the physics and fundamental-performance potential of various scaled mono-layer transition-metal-dichalcogenides and black-phosphorus (BP) MOSFETs down to a gate length of 5 nm, including the effect of electron-phonon scattering. Our study highlights the good scalability and drive-current potential of HfS2 and the impact of optical-phonon scattering for BP.**

Keywords— Semiconductor Physics, 2D-material, Quantum transport, DFT NEGF, CMOS

I. Introduction

Transition metal dichalcogenides (TMDs) or black phosphorus (BP), are widely investigated by the scientific community nowadays [1-3]. Their large variety of bandgaps, effective masses, and their excellent electrostatic properties related to their 2-D nature hold promise to find in their midst the candidate for ultra-scaled CMOS or post-CMOS applications. Full-band transport simulations including electron-phonon (e-ph) scattering have been shown crucial to consider intricate band-structure and transport effects [1] and assess the performance of these devices. Because there are many materials on which little is known, an *ab-initio* based quantum-transport method, such as DFT NEGF, is ideal for such novel device/material exploration.

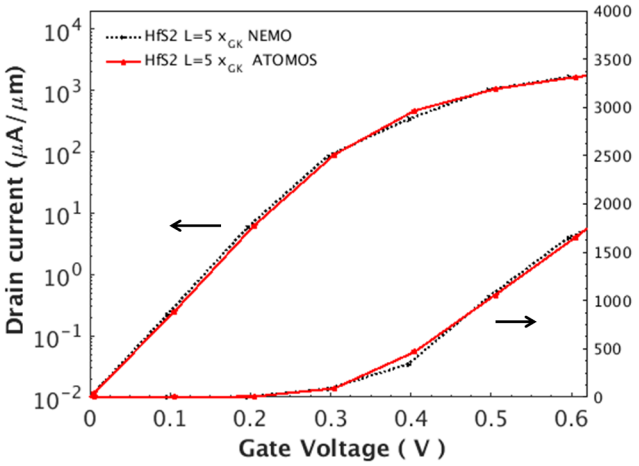

Fig. 1. $I_D(V_G)$ characteristics of a ballistic L = 5 nm HfS_2 nMOSFET (see schematic of Fig. 3) in the ΓK channel orientation simulated with DFT-NEGF using ATOMOS and NEMO5. V_{DD} = 0.5 V. I_{OFF} = 10 nA/µm.

Here, we report the development of a new DFT-NEGF based ATOmistic-MOdelling Solver (ATOMOS) and use it to assess the physics and fundamental-performance potential of various scaled mono-layers (1ML) TMD's and BP MOSFETs down to a gate length (L) of 5 nm, including the effect of e-ph scattering. Our results predict that the less-studied HfS_2 MOSFET has good scalability down to L = 5 nm with a promising high on-current (I_{ON}) level when oriented in the ΓM or ΓK directions. The 1ML BP-MOSFET I_{ON} is severely degraded by the intrinsic strong optical-phonon (OP) coupling that has been shown to appear in 1 or a few ML of free-standing BP [3]. It may, however, be possible to find a substrate that would attenuate the detrimental OP impact.

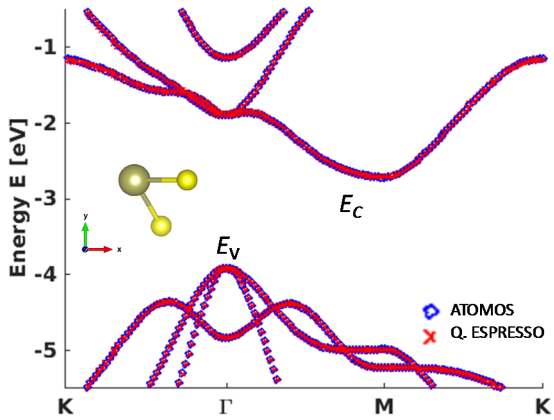

Fig. 2. Monolayer HfS_2 (1T-phase) band structure computed with QUANTUM ESSPRESSO using plane-wave DFT and with ATOMOS using the Wannierized Hamiltonian.

II. Solver Development

The core routines of ATOMOS were written for high-performance computing and computationally-demanding DFT Hamiltonians (H). They are based on C++ and multi-threaded MPI with various levels of parallelization.

Our Real-Space NEGF solver is based on the recursive-Green's function (RGF) algorithm [4]. A specific sparse block-matrix class, tailored for the RGF method, was developed to efficiently store H and other system matrices. Ultimately, the operation on the (slab) dense sub-block matrices are performed using BLAS and LAPACK. A dynamic scheduler, based on the master-slave approach, efficiently distribute the various energy-momentum (E-K) points between the different (MPI) ranks and ensure optimal load-balancing. A recursive adaptive-grid algorithm with global-error estimator is used for optimally generating the energy points. The contact-self energies are computed using the Sancho-Rubio method [5]. Electron-phonon scattering was considered using the self-consistent Born approximation [6]. For TMDs we used the DFT-computed e-ph parameters from [2], for BP those from [3]. To expedite the self-consistent Poisson-NEGF convergence, a predictor-corrector method [7] is used. To predict the carrier changes with respect to potential variation, various electron and hole functions, e.g., Fermi-Dirac integrals of order 0.5, 0, -0.5 [7], exponential, or their

978-1-7281-0940-4/19/$31.00 ©2019 IEEE

linearized versions have been implemented. A further adaptive-damping strategy for the charge or the potential can also be employed if necessary. We have used a DFT Hamiltonian that was expressed in a localized-orbital basis using the Wannierization technique [1]. ATOMOS finally embed Python to communicate with the outside world and get the user's inputs.

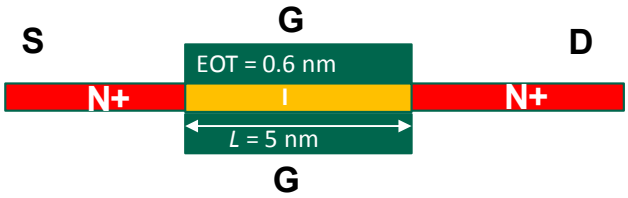

Fig. 3. Schematic view of an optimized 1ML DG nMOSFET.

The combination of state-of-the-art and fine-tuned algorithms with high-performance parallel computing leads to very fast and scalable computations. For the 2D devices simulated here, using a DFT-Hamiltonian including longer-range interactions and dissipative transport, the typical time for solving a single NEGF E-K point is typically ranging from a fraction of a second to a few seconds. On 200 cores, using the latest generation Intel Xeon CPU, the time to solve a single NEGF-Poisson loop bias point is of the order of tens of seconds to maximum a few minutes. A full IV curve is then typically achieved within about an hour to maximum a few hours on 200 cores.

The accuracy of our self-consistent NEGF simulator was also validated by comparing the drain current – gate voltage $I_D(V_G)$ characteristics of various devices, including a HfS_2 and BP MOSFETs, computed with ATOMOS and with the quantum-transport simulator NEMO5 [8] that we also augmented to use Wannierized H. Good agreement was achieved in all cases, as shown in Fig. 1 for the HfS_2 transistor.

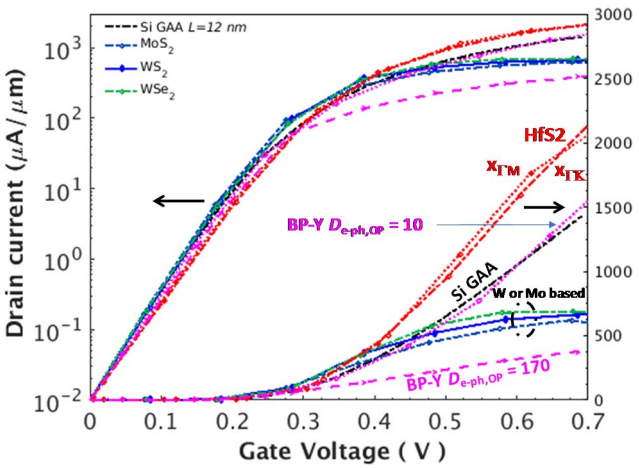

Fig. 4. $I_D(V_G)$ characteristics of the optimized L = 5 nm TMDs and BP-Y nMOSFETs , and the L = 12 nm Si GAA nMOS [12]. V_D = 0.5 V. I_{OFF} = 10 nA/µm. e-ph scattering is included. $D_{e\text{-}ph,OP}$ [eV/nm].

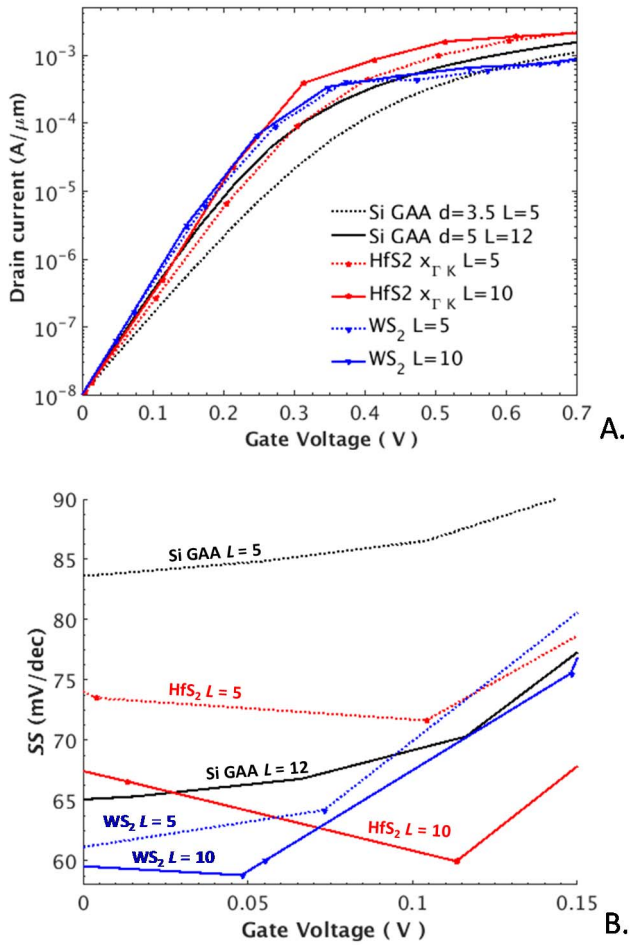

Fig. 5. $I_D(V_G)$ (A) and $SS(V_G)$ (B) characteristics of the WS_2 and HfS_2 nMOSFETs, as well as those of the Si GAA nMOS for different gate lengths as indicated in the legend (L is in nm). V_D = 0.5 V. I_{OFF} = 10 nA/µm. For the Si GAA, the diameter, d, (also indicated in nm in the legend) was optimized for each L.

III. DFT-Hamiltonian computation

To model the electronic states in the various TMD and BP monolayers, we used the density-functional theory (DFT)-based *ab-initio* tool QUANTUM ESSPRESSO [9]. The exchange-correlation functional OPTB86B [10] was used both in the geometry relaxation and in the computation of the electronic structure. The plane-wave cutoff energy and Monkhorst-Pack k-point grid values that were used in the relaxation and bandstructure calculations (without spin-orbit coupling) were chosen so that the total energy was well converged. The convergence criteria are set to less than 10^{-3} eV/Å forces acting on each ion and a total energy difference smaller than 10^{-3} eV between two subsequent iterations. To cut off the periodic image along the out-of-plane z-direction (Fig. 2), a vacuum layer of 20 Å was employed in the DFT simulations.

The Bloch wavefunctions are then transformed into maximally-localized Wannier functions (MLWF) typically centered on the ions using the wannier90 package [11]. Fig. 2 demonstrates the validity of our MLWF representation for the case of HfS_2. The resulting supercell information, including atoms and MLWF positions, lattice vectors, as well as the localized "tight-binding-like" Hamiltonian matrix elements, are then loaded into ATOMOS and used as building blocks to

create the full-device atomic structure and Hamiltonian matrix. The device geometry can be arbitrary rotated to a preferential channel orientation within the 2D layer. The device slab supercells typically encompass several conventional unit cells in the transport (x-axis) direction to keep, in the device Hamiltonian, the required Wannier Hamiltonian longer-range interactions (typically 12 to 15 Å). Periodic boundary conditions are assumed in the width (y-axis) direction and modeled with 16 k_y points. The longer-range interactions that extend to remote conventional cells in that direction are directly included in the periodic conditions.

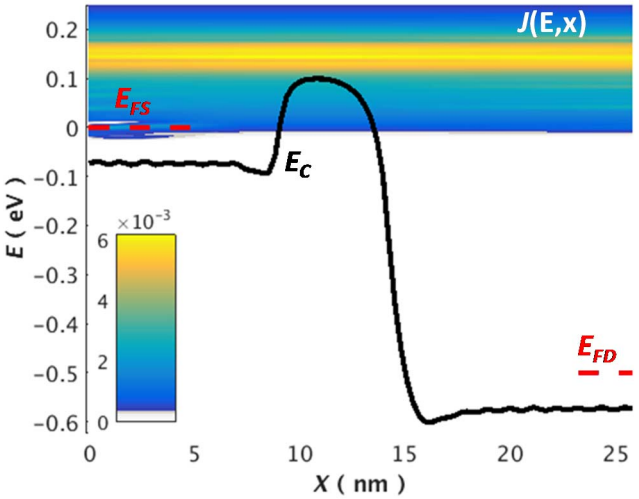

Fig. 6. Current spectrum *J(E, x)* (surface plot), as well as conduction-band (solid) edges along the channel direction, *x*, in off-state, for the L = 5 nm HfS_2 nMOSFET in the ΓK channel orientation with electron-phonon scattering. Source and drain Fermi-level positions are also indicated (red dash).

IV. RESULTS

The schematic of the studied 1ML double-gated (DG) nMOSFETs is shown in Fig. 3. Fig. 4 benchmarks the $I_D(V_G)$ characteristics of various L = 5 nm TMD and BP MOSFETs at a typical off-state leakage I_{OFF} = 10 nA/µm against that of an optimized Si gate-all-around nanowire (GAA) [12], but at relaxed gate length (L = 12 nm). For the Si GAA, scaling L below 10 nm typically results in subthreshold slope (*SS*) and I_{ON} degradation (Fig. 5), e.g., due to electrostatic control losses, quantum confinement and source-to-drain tunneling (SDT). On the contrary, for all the 2D materials shown on Fig. 4, we observed marginal I_{ON} degradation when scaling L down to 5 nm. However, as also reported in other studies [13], the most commonly studied TMDs, i.e., those having a W or Mo chalcogen metal, do not provide enough drive current for high-performance applications [14], and other materials with current level similar or higher than that of the L = 12 nm Si GAA are desired.

Fig. 5 shows with more details the impact of gate length scaling on $I_D(V_G)$ and $SS(V_G)$ characteristics for the WS_2 and HfS_2 MOSFETs as well as for the Si device. For the Si GAA, we optimized (scaled down to achieve best I_{ON}) the nanowire diameter from 5 to 3.5 nm when scaling L. Still, the atomistically-thin 2D transistors suffer less degradation than the GAA MOSFET. HfS_2 features more SS degradation (but better I_{ON}) than WS_2 when scaling L down to 5 nm. This is related to a mild but stronger SDT effect (Fig. 6) related to its better transport properties.

Overall, our results predict (Fig. 4) that the less-studied HfS_2 (in the octahedral (1T) phase) MOSFET has good scalability down to L = 5 nm and features a promisingly high on-current (I_{ON}) level, especially when oriented in the ΓM or ΓK directions. Fig. 6 gives more details about the impact of crystal orientation and electron-phonon (e-ph) scattering on the performance of the device. As expected by the short gate length and low values of the electron-phonon coupling in HfS_2, e-ph has only a limited impact on I_{ON}.

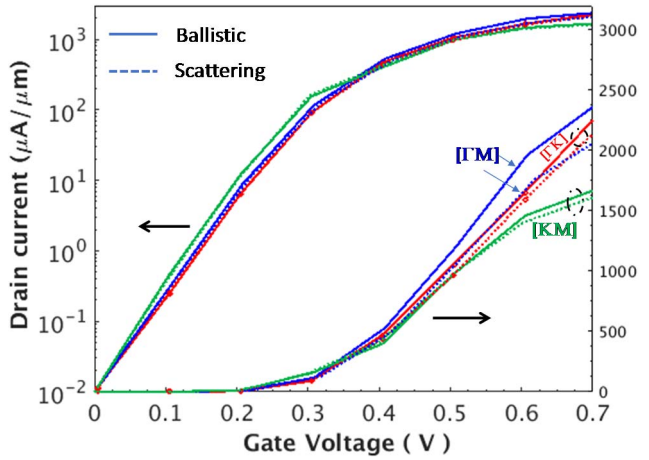

Fig. 7. $I_D(V_G)$ characteristics of the L = 5 nm HfS_2 nMOSFET for various channel orientations (ΓM, ΓK and KM) and scattering conditions (ballistic, with e-ph). V_D = 0.5 V. I_{OFF} = 10 nA/µm. HfS_2 with e-ph [2]: $D_{e\text{-}ph,AC}$ = 1.31 eV. $\hbar\omega_{OP}$ = 42 meV, $D_{e\text{-}ph,OP}$ = 9.9 eV/nm.

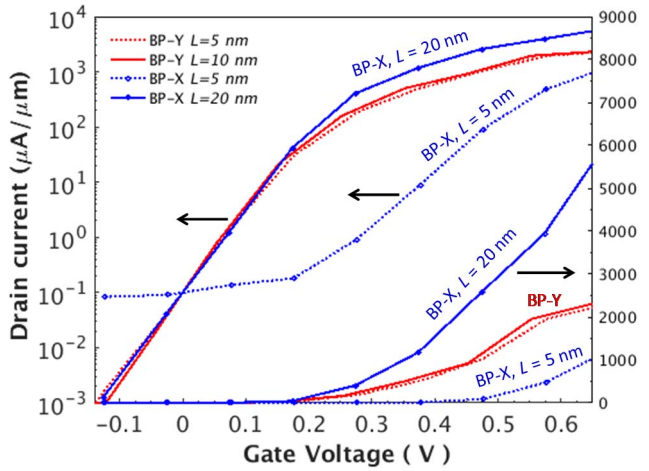

Fig. 8. $I_D(V_G)$ characteristics under ballistic approximation of the L = 5 and 10 nm BP-Y and L = 5 and 20 nm BP-X nMOSFETs. V_D = 0.5 V. I_{OFF} = 100 nA/µm.

Concerning, the 1ML BP-MOSFET, the ΓY channel orientation (BP-Y), i.e., the direction with the highest transport effective mass, was chosen as the L = 5 nm ΓX-oriented BP MOSFET characteristics were strongly degraded by SDT (Fig. 8 and Fig. 9). Owing to its very low transport effective mass, the BP-X device achieves the highest ballistic I_{ON} at relaxed gate length, but suffers more from SDT than BP-Y at scaled L. The cross-over point where I_{ON} BP-Y exceed BP-X is roughly around L =10 nm.

Most of the transport studies on scaled BP devices with 1ML or a few layers BP to date have been dealing either with ballistic performance or have neglected the optical-phonon coupling [15]. The 1ML BP-MOSFET I_{ON} is severely

degraded by the intrinsic strong optical-phonon (OP) coupling that is present in 1 or a few ML of BP ($D_{\text{e-ph,OP}}$ = 170 eV/nm for a free standing single monolayer) [3] (Fig. 5). As BP has a strong interlayer coupling, it may, however, be possible to find a substrate that would attenuate the detrimental OP impact. Our results show, however, that a very strong reduction of the optical coupling constant ($D_{\text{e-ph,OP}}$ < 20 eV/ nm) would be required to match the Si GAA I_{ON}. The existence of such a substrate is presently unclear.

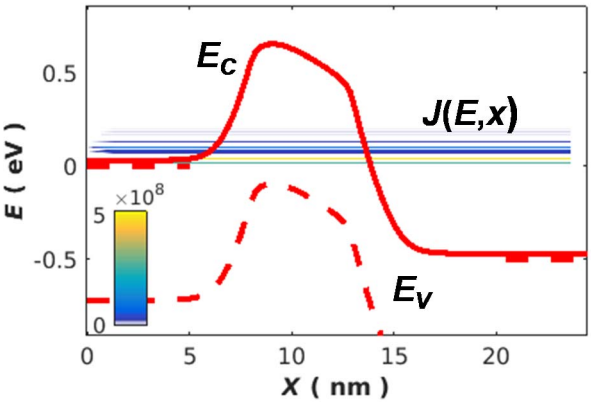

Fig. 9. Current spectrum *J(E, x)* (surface plot), as well as conduction-band (solid) and valence-band (dashed) edges along the channel direction, *x*, in off-state, for the *L* = 5 nm ballistic BP-X nMOSFET. Source and drain Fermi-level positions are also indicated (red dash).

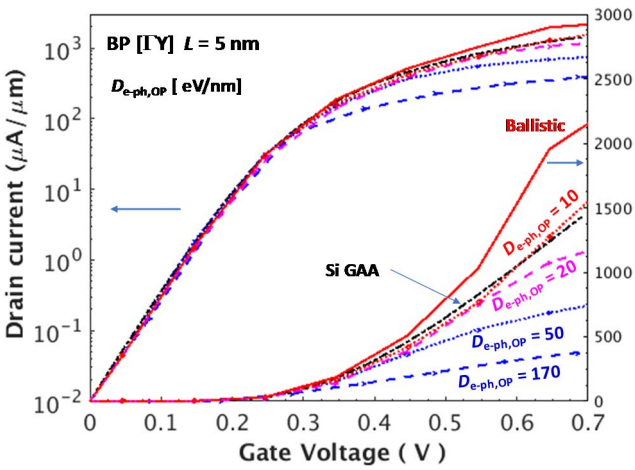

Fig. 10. $I_D(V_G)$ characteristics of the *L* = 5 nm BP-Y nMOSFET for different scattering strengths and the *L* = 12 nm Si GAA nMOS. V_D = 0.5 V. I_{OFF} = 10 nA/μm. BP-Y with e-ph [3]: $D_{\text{e-ph,AC}}$ = 7.11 eV. •ω_{OP} = 32 meV, $D_{\text{e-ph,OP}}$ as indicated in the figure ($D_{\text{e-ph,OP}}$ = 170 eV/nm for a free standing 1ML).

V. Conclusions

A state-of-the-art DFT-NEGF based ATOmistic-MOdelling Solver (ATOMOS) was developed and used to assess the physics and fundamental-performance potential of various scaled mono-layers TMD's and BP MOSFETs down to a gate length of 5 nm, including the effect of e-ph scattering. Our results predict that the less-studied HfS_2 MOSFET has good scalability down to *L* = 5 nm with a promising high on-current (I_{ON}) level when oriented in the ΓM or ΓK directions. The 1ML BP-MOSFET I_{ON} is severely degraded by the intrinsic strong optical-phonon (OP) coupling that appears in 1 or a few ML of free-standing BP. It may, however, be possible to find a substrate that would attenuate the detrimental OP impact.

References

[1] Á. Szabó, R. Rhyner, and M. Luisier, "Ab initio simulation of single- and few-layer MoS2 transistors: Effect of electron-phonon scattering", Phys. Rev. B 92, 035435, 2015. Doi: 10.1103/PhysRevB.92.035435.

[2] Z. Huang, W. Zhang and W. Zhang, "Computational Search for Two-Dimensional MX2 Semiconductors with Possible High Electron Mobility at Room Temperature", Materials, vol. 9, no.9, p. 716, 2016. Doi: 10.3390/ma9090716.

[3] G. Gaddemane, W. G. Vandenberghe, M. L. Van de Put, S. Chen, S. Tiwari, E. Chen, M. V. Fischetti, "Theoretical studies of electronic transport in mono- and bi-layer phosphorene: A critical overview", Phys. Rev. B, vol. 98, p. 115416, 2018. DOI:10.1103/PhysRevB.98.115416.

[4] A. Svizhenko, M. Anantram, T. Govindan, R. Biegel, R. Venugopal, "Two-dimensional quantum mechanical modeling of nanotransistors", J. Appl. Phys. 91, 2343–2354 (2002).

[5] M. Sancho, J. Sancho, J. Sancho, and J. Rubio, "Highly Convergent Schemes for the Calculation of Bulk and Surface Green Functions", J. Phys. F: Met. Phys., vol. 15, pp. 851-858, 1985.

[6] A. Afzalian, "Computationally Efficient self-consistent Born approximation treatments of phonon scattering for Coupled-Mode Space Non-Equilibrium Green's Functions", J. Appl. Phys., vol. 110, p. 094517, 2011. Doi: 10.1063/1.3658809.

[7] A. Trellakis and A.T. Galick, "Iteration scheme for the solution of the two-dimensional Schrödinger-Poisson equations in quantum structures", J. of Applied Physics, vol. 81, p. 7880, 1997. Doi: 10.1063/1.365396.

[8] S. Steiger, M. Povolotskyi, H.-H. Park, T. Kubis and G. Klimeck, "NEMO5: A Parallel Multiscale Nanoelectronics Modeling Tool", IEEE TNANO, vol. 10, p. 1464, 2011. Doi: 10.1109/TNANO.2011.2166164.

[9] Paolo Giannozzi; Stefano Baroni; Nicola Bonini; Matteo Calandra; Roberto Car; Carlo Cavazzoni; Davide Ceresoli; Guido L Chiarotti; Matteo Cococcioni; Ismaila Dabo; Andrea Dal Corso; Stefano de Gironcoli; Stefano Fabris; Guido Fratesi; Ralph Gebauer; Uwe Gerstmann; Christos Gougoussis; Anton Kokalj; Michele Lazzeri; Layla Martin-Samos; Nicola Marzari; Francesco Mauri; Riccardo Mazzarello; Stefano Paolini; Alfredo Pasquarello; Lorenzo Paulatto; Carlo Sbraccia; Sandro Scandolo; Gabriele Sclauzero; Ari P Seitsonen; Alexander Smogunov; Paolo Umari & Renata M Wentzcovitch (2009). "QUANTUM ESPRESSO: a modular and open-source software project for quantum simulations of materials". Journal of Physics: Condensed Matter. 21 (39): 395502. berg. pp. 155–178. Doi:10.1007/978-3-642-61478-1_10.

[10] J. Klimeš, D. R. Bowler, and A. Michaelides, "Chemical accuracy for the van der Waals density functional", J. Phys.: Cond. Matt. 22, 2, 022201 (2010). Doi: 10.1088/0953-8984/22/2/022201.

[11] A.A. Mostofi, J.R. Yates, G. Pizzi, Y.S. Lee, I. Souza, D. Vanderbilt, N. Marzari, "An updated version of wannier90: A tool for obtaining maximally-localised Wannier functions", Comput. Phys. Commun. 185, 2309 (2014). Doi:10.1016/j.cpc.2014.05.003.

[12] A. Afzalian, M. Passlack and Y.-C. Yeo, "Scaling perspective for III-V broken gap nanowire TFETs: An atomistic study using a fast tight-binding mode-space NEGF model", in Proc. IEEE Int. Electron Device Meeting (IEDM), San-Francisco, CA, USA, 2016, pp. 30.1.1-30.1.4. Doi: 10.1109/IEDM.2016.7838510.

[13] M. Luisier, A. Szabo, C. Stieger, C. Klinkert, S. Brück, A. Jain, L. Novotny, "First-principles simulations of 2-D semiconductor devices: Mobility, I-V characteristics, and contact resistance", in Proc. IEEE Int. Electron Device Meeting (IEDM), San-Francisco, CA, USA, 2016, pp. 5.4.1-5.4.4. DOI: 10.1109/IEDM.2016.7838353.

[14] https://irds.ieee.org/roadmap-2017.

[15] K.-T. Lam, S. Luo, B. Wang, C.-H. Hsu, A. Bansil, H, Lin, G. Liang, "Effects of interlayer interaction in van der Waals layered black phosphorus for sub-10 nm FET", in Proc. IEEE Int. Electron Device Meeting (IEDM), San-Francisco, CA, USA, 2015, pp. 12.2.1-12.2.4. DOI: 10.1109/IEDM.2015.7409681.